Int J Adv Manuf Technol (2007) 33: 1087–1096
DOI 10.1007/s00170-006-0556-9

ORIGINAL ARTICLE

Tian-Ming Wang · Jun-Tong Xi · Ye Jin

A model research for prototype warp deformation in the FDM process

Received: 2 June 2005 / Accepted: 4 February 2006 / Published online: 14 April 2006

Abstract In rapid prototyping (RP) technology, prototypes are constructed by the sequential deposition of material layers. When the deposition process involves temperature gradients, thermal stresses will develop. In this paper, the prototype deformation in fused deposition modeling (FDM) processes is studied, and the essence of the deformation and the interacting principles are analyzed. According to basic hypotheses and simplifications, the mathematical model of the prototype warp deformation is constructed, and each of the influencing factors concretely, including the deposition layers number n, the stacking section length L, the chamber temperature T_e, and the material linear shrinkage rate α, is quantificationally analyzed. Based on the analysis results, some issues and phenomena in the FDM process are rationally explained. Furthermore, the improving methods for the reduction of the prototype warp deformation are proposed, and the applying effect is better.

Keywords Rapid prototyping · Fused deposition modeling · Warp deformation · Thermal stress

1 Introduction

Rapid prototyping (RP), also called layer manufacturing (LM), has been successfully employed in several industries to fabricate concept models, prototypes, and even functional parts. The principle underlying RP is that the original 3D geometrical part is decomposed into 2D profile layers. Then, the material is increased layer-by-layer for most RP processes, rather than by removing material, as in machining processes. Hence, complex geometrical parts can be fabricated automatically and rapidly, and the associated fixture and tooling are not required because the RP process is automated from the computer-aided design (CAD) program to the prototyping system.

With the development of RP technology, the industry and universities have developed a number of RP processes. One category is the fused deposition (FD) based solid freeform fabrication process; fused deposition modeling (FDM) falls into this category. As one of the most promising RP techniques in terms of dimensional accuracy, speed, and cost-effectiveness, FDM has been widely used. The process utilizes the simple idea of the melting, extrusion, and resolidification of thermoplastic materials. As the nozzle controlled by computer is moved over the x–y worktable, it deposits a thin bead of extruded plastic with high temperature to form a road. The fusing and welding interfaces of polymer roads side-by-side in a raster configuration produces each layer, and form layer-by-layer to produce a prototype.

In FDM, inner stresses resulting from the contraction of deposition fibers within one layer can affect the prototype size precision, bring about prototype deformation, including warp and inner-layer delaminating or cracking, destroy the supporting structures between the main body of the prototype and the worktable, and even cause fabrication failure. In other RP processes, similar quality issues of warp deformation also widely exist. Many researchers have investigated the inner stresses. Jayanthi et al. [1] discussed how the scanning pattern of the laser in stereolithography (SLA) influences the resulting deflection of the part. Yang et al. [2] studied the effect of residual stresses and researched the method of shrinkage compensation in metal prototypes fabricated by selected laser sintering (SLS). Nickel et al. [3] investigated the metal parts produced using shaped deposition manufacturing (SDM). Through finite element modeling and experimentation, they determined that substrate preheating and rigid bolting of the substrate could reduce the resulting part distortion. In addition, Sonmez and Hahn [4] proposed the modeling of

T.-M. Wang (✉) · J.-T. Xi · Y. Jin
Institute of Computer Integrated Manufacturing,
School of Mechanical and Power Engineering,
Shanghai Jiaotong University,
Room 1205, HaoRan Building, No. 1954, HuaShan Road,
Shanghai, 200030, People's Republic of China
e-mail: wangtianming@sjtu.edu.cn
Tel.: +86-21-52541501
Fax: +86-21-52541501
e-mail: jtxi@sjtu.edu.cn
e-mail: jinye@sjtu.edu.cn

thermo-mechanical behavior during the laminated object manufacturing (LOM) process. Based on the finite element method, heat transfer and stress analyses were carried out.

How to obtain the high fabrication quality of the prototype is one of the most important problems in the RP technology field [5]. Reducing the warp deformation and improving the shaping precision of the prototype are also the research emphases in this field. Thus, one specific analyzing model of warp deformation is necessary to be established, since the FDM process has its own characteristics. Based on the model, the influencing factors of warp deformation can be quantificationally studied. Some methods can be proposed to reduce and eliminate the FDM prototype deformation. According to the analyzing conclusions, some measures for improving the prototype quality can be used to direct prototype fabrication. Furthermore, the analyzing methods and some analysis results are also important references for other RP processes.

2 Mathematical model of prototype warp deformation in the FDM process

A commercial FDM machine consists, essentially, of a head system attached to a carriage moving in the horizontal x–y plane. The head system commonly adopts the double-nozzle structure: one nozzle extrudes modeling materials for fabricating the body of the prototype and the other extrudes secondary materials for fabricating the structures to support any overhanging section of the prototype. These two nozzles alternately work until the prototype has been finished. The function of the head-liquefier assembly is to heat and pump the filament material through the tip onto the prototype surface. The spooled filaments are fed into the liquefier via a set of two freewheels driven in a counter rotating fashion, which provides enough torque to the filaments to act as a piston during the extrusion phase. The filaments are softened and melted inside the liquefier, and are then extruded out of a nozzle tip located at the bottom end of the liquefier. On the special fabricating conditions, the extruded fiber is deposited along the appointed path.

2.1 Basic hypotheses and simplifications

The amorphous thermoplastic fiber extruded from a nozzle tip was then deposited on the worktable. Before constructing the analytical model of the prototype warp deformation, it is necessary to simplify the deposition process of FDM, so, reasonable hypotheses are proposed. The basic hypotheses and simplifications are listed as the following:

1. The high-temperature fiber extruded out of the nozzle will be deposited on a worktable following the scheduled road path. When cooling from the melted temperature T_m to the glass-transition temperature T_g, the deposited thermoplastic fiber can be subjected to contraction. However, when the cooling temperature ranges between T_m and T_g, the deposited fiber can acquire a larger deformation with less force, and the capacity to resist outside force is small [6]. Therefore, in spite of the contraction, the inner stresses of the deposited fiber are not accumulated. The inner stress is mainly produced in the course of the cooling temperature changing from the glass-transition temperature T_g to the chamber temperature T_e.
2. The extruded high-temperature fiber is cooling rapidly. For the ABS P400 material as an example, it takes approximately 0.55 s to cool from the melting temperature of 270°C to the glass-transition temperature of 94°C when it is extruded out of a nozzle with a diameter of 0.254 mm, and it takes about 1.20 s to cool from the glass-transition temperature to 94°C to the chamber temperature of 70°C [7]. But for the movement head with a speed of 30 mm/s, the time for finishing a layer of a middle-size prototype is much longer than the fiber cooling time. So, the temperature of the layer that is being deposited is considered to be equal to the temperature of the layers that have been finished, and the temperature accords with the chamber temperature T_e. In addition, the just-extruded fiber retains the temperature of the nozzle, without any heat loss.
3. The prototype deformation results from the release of the inner stresses. The warp deformation is the deformation summation of the side-by-side and the layer-by-layer deposited fibers. For analysis convenience, it is necessary to simplify the deposition process in advance. Each filling layer is considered as a flat plane, and every layer has been finished depositing instantaneously. When analyzing the fiber-by-fiber deformation in a concrete layer, it is supposed that the layer is closely deposited along a zig-zag path, and that there is no void between stacking fibers.

2.2 Foundation of the mathematical model of warp deformation

The inter-layer deformation and the intra-layer deflection all result from the contraction of the deposited fibers, and they can also affect each other. The inter-layer deformation is the stacking deformation of each layer along the vertical direction of the deposition plane, so it is also called warp deformation. The intra-layer deformation is mainly the side deflection of deposited fibers in the deposition layer. Due to the stacking interlacement of the inter-layer raster roads, the intra-layer side deflection and twist of the prototype can be basically counteracted. To sum up, the contraction of the deposited fibers induces the prototype deformation, and the inter-layer warp deformation is the primary deformation.

2.2.1 Inter-layer deformation model

According to hypothesis 1, there do not exit any stress inside newly deposited fibers which are cooling from the extruded temperature T_0 to the glass-transition temperature T_g. The inner stresses of the fibers are mainly produced in

the following process of the fibers' temperature changing from the glass-transition temperature T_g to the chamber temperature T_e. The overall analyzing process of warp deformation is shown in Fig. 1. It is supposed that newly deposited layer freely contracts with cooling, and that the layer is separated from the other layers of the prototype. Figure 1b shows the schematic diagram. In the process of cooling to the chamber temperature T_e, the thin separated layer contracts uniformly and no stresses develop. The stress and strain of the separated thin layer is given by $\sigma=0$ and $\varepsilon=\alpha\Delta T$, where ΔT is the change of temperature during the cooling process and α is the linear shrinkage coefficient. The next step in the thought experiment is, while at chamber temperature T_e, to strain the thin layer back to their original length (Fig. 1c). This step produces a strain given by $\varepsilon=-\alpha\Delta T$ and a stress given by $\varepsilon=-E\alpha\Delta T$, where E is the Young's modulus of the deposited materials. The last step in the thought experiment is to re-attach the new thin layer to the main body and enforce the equilibrium conditions (Fig. 1d). The inner stresses of the newly deposited layer due to contraction can act on the other layers of the prototype. To satisfy the condition of the summation of the forces being equal to zero, a constant stress σ^* is added to the stress state.

According to hypothesis 3, suppose the extruded ABS fibers are linear-elastic and isotropic, and that there is perfect bonding between the fibers. Therefore, each filling layer of the FDM prototype is considered as a flat plane. Each flat plane of stacking layers is composed of many side-by-side deposited fibers with approximate rectangular cross-sections, and there is no void between deposited fibers. The cooling deposited fibers will contract along the direction of the deposition paths. Due to the fibers having the uniform material, the same cross-section shape, and constant and steady deposition speed, the stress inside each deposited fiber of the layer plane may be considered as a uniform stress. If the fibers of the layers of one prototype are deposited with different and unsteady speeds, the heat gain of the prototype body in unit time will change. So, the cooling speed of the fibers can also change, and the temperature distribution of the depositing layer will be disturbed (see Fig. 2). In Fig. 2, every layer in the simulation analyses is composed of three deposited fibers, and the fibers all have the horizontal section with size 0.0005 m×0.12 m. Each layer has been deposited respectively with different speeds. Due to the different depositing speeds, the temperature distribution of each layer is different, as shown in Fig. 2. The stress in each deposited fiber can be influenced by the different cooling speed to a certain extent. So, the differences of the stress in the layers will be produced by the different depositing speeds. However, if the speed of the deposited fibers in the prototype is constant all the time, the stresses in every layer plane can be considered as a uniform stress. The FDM

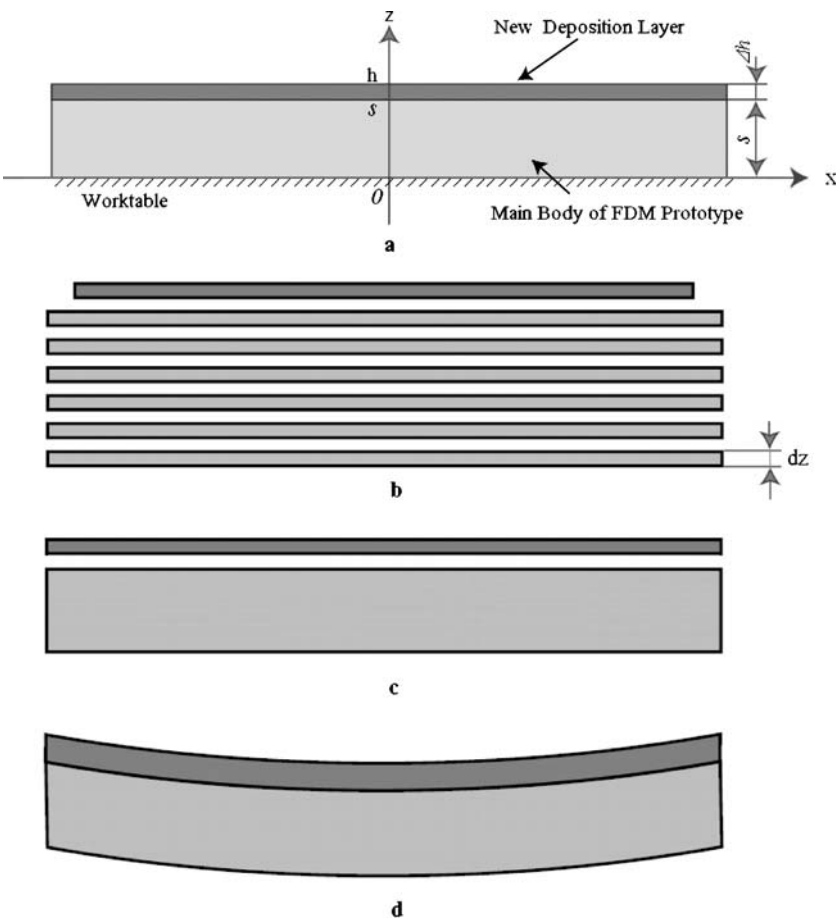

Fig. 1a–d Analysis process of thermal stress thought experiment. **a** Initial state. **b** Detach layers and let them cool to the chamber temperature. **c** Strain layers back to the original length. **d** Reattach layers and enforce equilibrium conditions

prototype is generally fabricated with a constant speed in the chamber of the FDM machine. In addition, each deposition fiber in every new layer plane has the same state of being restricted, so a constant stress σ^* is added to the stress state in the analyzing process of the warp deformation.

This stress represents the uniform change in stress that occurs in the layers during the cooling time. In addition, the net force of the prototype body is equal to zero. To satisfy equilibrium, the net moment must also be zero. To achieve no net moment, a pure bending stress, $E(z-d)/R$, is added to the stress state, where d is the position of the neutral axis and R is the radius of curvature. The stress represents the linear change that occurs as the layers cool to chamber temperature. The final stress state in the main body of the prototype is given by:

$$\sigma = -E\alpha\Delta T + \sigma^* + \frac{E(z-d)}{R} \tag{1}$$

$$\varepsilon = \frac{\sigma^*}{E} + \frac{z-d}{R} \tag{2}$$

where ε is the thermal strain, σ is the thermal stress, α is the linear shrinkage coefficient, E is the Young's modulus of the deposited materials, d is the position of the neutral axis, R is the radius of curvature, T_g is the glass-transition temperature of the deposited materials, T_0 is the extruded temperature, T_e is the chamber temperature, σ^* is a constant stress which is added to the stress state to satisfy condition of the summation of the forces equaling zero, and ΔT is the change of temperature from T_g to T_e.

According to hypothesis 1 and hypothesis 2, ΔT is a step function is given by:

$$\Delta T = \begin{cases} T_g - T_e & s \le z \le h \\ 0 & 0 \le z \le s \end{cases} \tag{3}$$

For the depositing prototype, in addition to the net force being equal to zero, the net moment is also zero. The summation of the forces and the moments are described in Eqs. 4 and 5:

$$\int_0^h \left(-E\alpha\Delta T + \sigma^* + \frac{E(z-d)}{R}\right)dz = 0 \tag{4}$$

$$\int_0^h \left(-E\alpha\Delta T + \sigma^* + \frac{E(z-d)}{R}\right)z\,dz = 0 \tag{5}$$

The radius of curvature R must be solved first before calculating the warp deformation. There are only two equilibrium equations (Eqs. 4 and 5) that can be used to solve for the unknowns, but there are three unknowns: σ^*, d, and R. Notice, however, that both σ^* and Ed/R are constants and can be combined to form one unknown σ', as follows:

$$\sigma' = \sigma^* - \frac{Ed}{R} \tag{6}$$

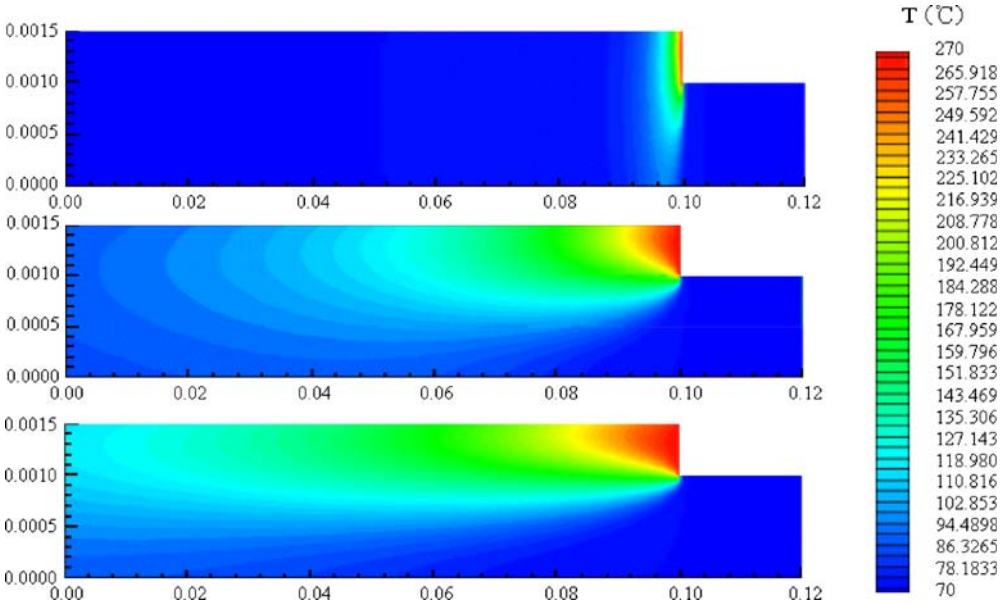

Fig. 2a–c Evolution of the temperature distribution in the deposited fibers with different depositing speeds. **a** 5 mm/s. **b** 20 mm/s. **c** 40 mm/s

So now there are two equations of Eqs. 7 and 8 and two unknowns of σ' and R:

$$\int_0^h \left(-E\alpha\Delta T + \sigma' + \frac{Ez}{R}\right)dz = 0 \tag{7}$$

$$\int_0^h \left(-E\alpha\Delta T + \sigma' + \frac{Ez}{R}\right)zdz = 0 \tag{8}$$

Equations 3, 7, and 8 can be used to solve for the curvature k:

$$k = \frac{1}{R} = \frac{6\alpha}{h}(T_g - T_e)\left(1 - \frac{s}{h}\right)\frac{s}{h} \tag{9}$$

The difference between h and s is Δh, where Δh is the thickness of every deposited layer. For the prototype composed of n deposited layers, the equation, $s/h=(n-1)/n$ is obtained. Therefore, Eq. 9 can be converted into Eq. 10, as follows:

$$\begin{aligned} k = \frac{1}{R} &= \frac{6\alpha}{h}(T_g - T_e)\left(1 - \frac{n-1}{n}\right)\frac{n-1}{n} \\ &= \frac{6\alpha}{n\Delta h}(T_g - T_e)\frac{n-1}{n^2} \end{aligned} \tag{10}$$

The warp deformation δ can be determined from the radius of curvature R, as shown in Fig. 3. L is the stacking layers' section length:

$$R\beta = \frac{L}{2}, \quad \textit{and} \quad \cos\beta = \frac{R-\delta}{R} \tag{11}$$

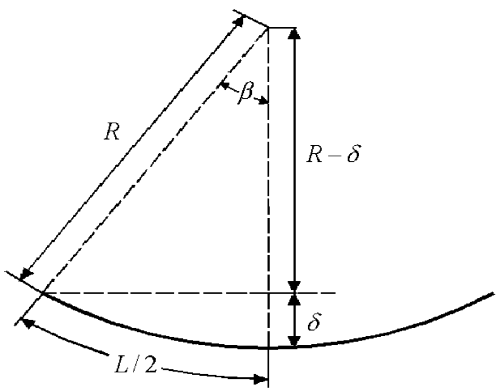

Fig. 3 Relationship between warp deflection and the radius of curvature

Combining Eqs. 10 and 11, finally, the equation of the inter-layer warp deformation is obtained:

$$\begin{aligned} \delta = R\left(1 - \cos\frac{L}{2R}\right) &= \frac{n^3\Delta h}{6\alpha(T_g - T_e)(n-1)} \\ &\times \left\{1 - \cos\left[\frac{3\alpha L}{n\Delta h}(T_g - T_e)\frac{n-1}{n^2}\right]\right\} \end{aligned} \tag{12}$$

In Eq. 12, L is the section length of the stacking layers, δ is the warp deformation of the prototype, R is the radius of curvature, n is the number of layers that have been deposited, and Δh is the thickness of every deposited layer.

2.2.2 Intra-layer deflection analysis

According to hypothesis 3, the total deformation due to the release of thermal stresses is the summation of the intra-layer deflection and the inter-layer deformation. Therefore, before analyzing the total deformation model of the prototype, the intra-layer deflection and the inter-layer deformation need to be respectively analyzed in advance. The inter-layer warp deformation of the prototype has been obtained as in Eq. 12.

As for analyzing the intra-layer deflection, each filling layer is considered as a flat plane, and every layer plane has been deposited instantaneously. In addition, the layer is closely deposited with the melted fiber following a zig-zag path, and there is no void between fibers. So, the whole analysis process is very similar to the analysis of inter-layer warp deformation. The inter-layer deformation equations are suitable for the intra-layer analysis.

Currently, three kinds of deposition methods are used for intra-layer filling. These are raster (zig-zag), contour, and contour/raster combination, as shown in Fig. 4. For raster deposition, the whole path can usually be laid in one single motion of the nozzle. This speeds up the deposition process; however, rotation in the tool direction would only slow it down slightly. Raster paths usually suffer from inaccuracies in deposition and bad surface quality. In the contour filling method, however, the boundary of a layer is successively offset until it fills the entire domain. This method fits the boundary well, and has good surface quality. Conversely, it yields a set of distinct paths that need to be traversed to deposit all of the material. Distinct paths have to be indexed and properly positioned to start and finish each contour path. As a result, the deposition process is slow. The combination of the contour and raster methods employs contours to fit the boundaries and raster to fill inside them. It yields good surface quality with a short build time.

Thus, the raster/contour deposition strategy is used in the model analysis and the fabrication of the prototypes in this research. To improve the prototype strength and decrease the anisotropy of the prototype, the extruded fiber is generally deposited along the road path as shown in Fig. 5, and the discrete raster angles of ±45° between adjacent

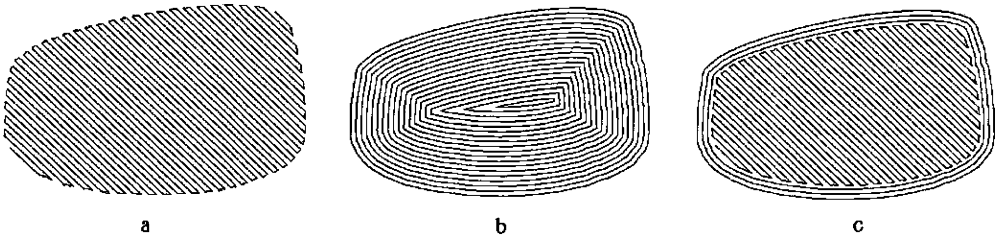

Fig. 4a–c Different in-layer deposition strategies of FDM. **a** Raster. **b** Contour. **c** Contour/raster

layer planes are considered. Road paths of adjacent deposition layers are interlaced. In addition, the deposition direction along the road path in every layer is also completely different. With the help of these deposition strategies, the side deflection of layers can be basically counteracted each other. Therefore, the side deflection to influence the total deformation cannot be taken into account in the deformation analysis.

3 Analyses of the mathematical model of warp deformation

From the mathematical model of the inter-layer warp deformation, it can be found that the influencing factors certainly include the deposition layer number n, the stacking section length L, the material linear shrinkage rate α, the chamber temperature T_e, and the glass-transition temperature T_g. These factors interplay and jointly influence the warp deformation of the FDM prototype.

The material of ABS P400 is used for the analyses of the mathematical model. The filament of ABS P400 was developed by Stratasys Inc., and this filament is widely used by most FDM machines. Compared with other thermoplastic materials, the material possesses better characteristics, including wide melting scope (105°C~290°C), low shrinkage rate (0.3%~0.5%), strong thermal–chemical stability, and high strength. Some prototypes fabricated with the material can be used as the functional parts.

In general, the physical parameters of ABS P400 material include glass-transition temperature T_g=94°C, solid density p=1,050 kg/m^3, and Young's modulus E=2,230 MPa. As the defaults of the FDM2000 machine, the extrusion temperature T_0=270°C, the chamber temperature T_g=70°C, and the nozzle of T_{10} type with a diameter of 0.254 mm are usually adopted for most fabrication process requirements [8].

According to the physical parameters of the ABS P400 material and the working parameters of the FDM2000 machine, each influencing factor is quantitatively analyzed. These detailed analysis of processes are as follows.

3.1 Influence of the layers number n on the warp deformation

Figure 6 shows three curves of the maximal warp deformation in relation to the deposition layers number with the stacking section length L=40 mm, 70 mm, and 100 mm, respectively. This figure shows that the warp deformation is rapidly reduced with the number of deposition layers increasing at the very start. When the layers number n reaches 70, the decreasing tendency of the warp deformation becomes slow with the layers number increasing in succession. This conclusion is helpful to direct the rational selection of the layers number and the stacking section length before small prototypes are ready to be fabricated. In addition, it can also be found from Fig. 6 that the longer the stacking section length, the bigger the warp deformation.

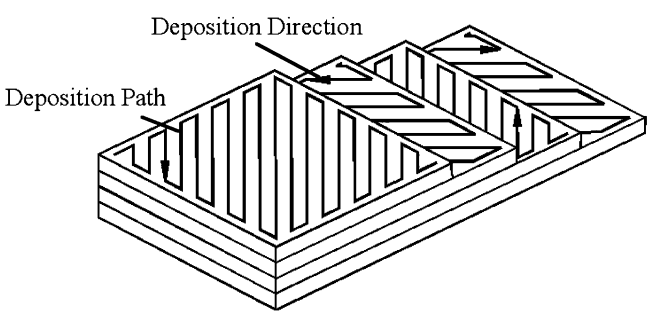

Fig. 5 Deposition paths and deposition directions of intra-layer roads

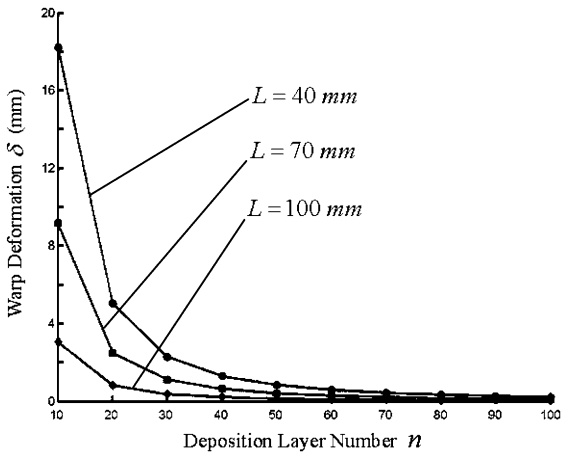

Fig. 6 Influence of the number of deposition layers n on the warp deformation of the prototype

3.2 Influence of the stacking section length L on the warp deformation

Figure 7 shows three curves of the maximal warp deformation in relation to the stacking section length with the deposition layers numbers of n=40, 70, and 100, respectively. From Fig. 7, it can be seen that the warp deformation moderately increases with the increase of the stacking section length, and this increasing tendency becomes bigger with the stacking section length continuously increasing. Therefore, in the FDM process, the selection and partition of deposition areas can effectively reduce the stacking section length L. In addition, Fig. 7 shows that the increasing tendency of warp deformation becomes bigger with increasing deposition layers number.

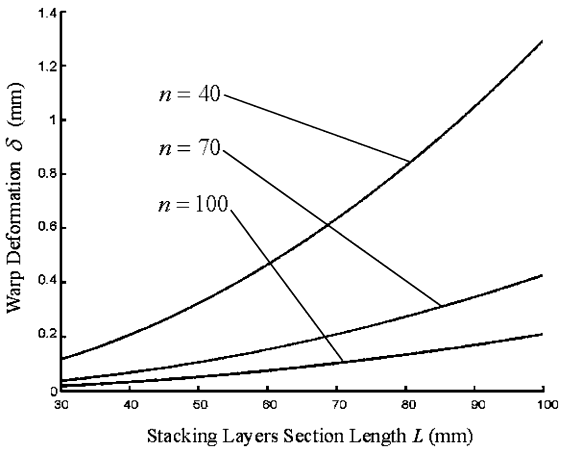

Fig. 7 Influence of the stacking section length L on the warp deformation of the prototype

3.3 Influence of the layers number n and stacking section length L on the warp deformation

If the warp deformation δ remains constant, the relationship between the deposition layers number n and the stacking section length L is linear. Figure 8 shows four lines of the stacking section length in relation to the deposition layers number with the warp deformations δ=0.1 mm, 0.4 mm, 1.0 mm, and 1.6 mm, respectively. To each given warp deformation δ, if each line slope can be solved with the condition of α=0.004 and T_g=70°C, a group of numerical values regarding the ratio of the stacking section length L to the deposition layers thickness $n\Delta h$ can be acquired (see Table 1). According to the allowable maximal warp deformation for selecting an appropriate ratio value in Table 1, the selected ratio is used as a standard to choose the depositing direction of the road path and to partition the filling areas of each layer.

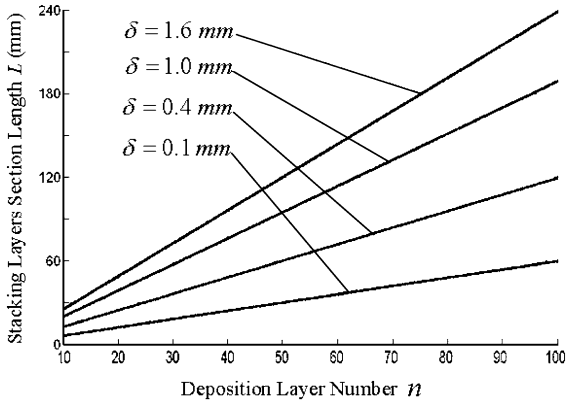

Fig. 8 Joint influence of the number of deposition layers n and the stacking section length L on the warp deformation

3.4 Influence of the chamber temperature T_e on the warp deformation

With the conditions of linear shrinkage coefficient α=0.004 and stacking section length L=70 mm, and varying chamber temperature T_e from 40°C to 90°C, Fig. 9 shows three curves of the warp deformation in relation to the chamber temperature with the deposition layers number n=40, 70, and 100, respectively. It can be seen that the warp deformation linearly decreases with increasing chamber temperature. When the chamber temperature T_e reaches the glass-transition temperature, the deformation becomes zero. So, it is helpful to reduce the warp deformation when the chamber temperature is rising. However, when the chamber temperature T_e is continually rising, the solidifying time of the deposited fiber will be prolonged, which may influence the quality of the depositing layer, due to the surface of deposited fibers having not entirely solidified. For the given material, the chamber temperature T_e has an optimal value, and this value needs to be chosen with real experiments. For the material of ABS P400, 70°C as the chamber temperature is usually adopted.

Table 1 Ratio of the stacking section length L to the deposition layers' thicknesses $n\Delta h$ with different definite values of warp deformation δ

δ (mm)	L(mm)/n	$L/n\Delta h$
0.1	0.596944	2.3502
0.2	0.844208	3.3237
0.4	1.193895	4.7004
0.6	1.462223	5.7568
0.8	1.688436	6.6474
1.0	1.887735	7.4320
1.2	2.067918	8.1414
1.4	2.233615	8.7938
1.6	2.387844	9.4010
1.8	2.532701	9.9713

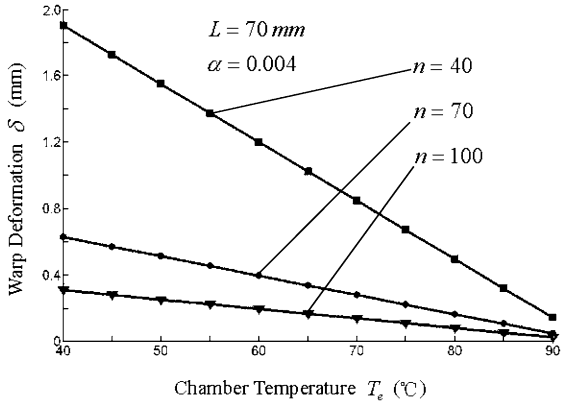

Fig. 9 Influence of the chamber temperature T_e on the warp deformation of the prototype

3.5 Influence of the material shrinkage rate α on the warp deformation

With the conditions of chamber temperature T_e=70°C and stacking section length L=70 mm, and varying material linear shrinkage rate α from 0.001 to 0.01, Fig. 10 shows three curves of the warp deformation in relation to the material linear shrinkage rate with the deposition layers number n=40, 70, and 100, respectively. It can be seen that the warp deformation linearly increases with increasing material linear shrinkage rate. Therefore, the material with a lower linear shrinkage rate is better for the FDM process.

4 Measures for the reduction of warp deformation

From the above analyses, two conclusions can be drawn for the reduction of warp deformation in the FDM process.

4.1 Materials

As seen from Eq. 3 and Fig. 10, the glass-transition temperature and the linear shrinkage rate of thermoplastic materials can directly influence the warp deformation. So, some concrete measures can be used for a special material to decrease its glass-transition temperature and linear shrinkage rate. It is helpful for the reduction of warp deformation.

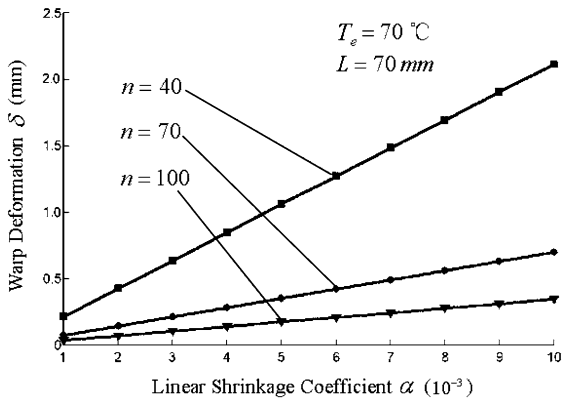

Fig. 10 Influence of the material linear shrinkage rate α on the warp deformation of the prototype

4.2 Process planning

(1) It can be seen from Figs. 7 and 8 that the size of the prototype is very important. The bigger the size of the prototype, especially the longer stacking section length, the larger the warp deformation. So, the prototypes with bigger size and thinner walls, in principle, should not be allowed to be fabricated by the FDM process.

In the fabrication process, a phenomenon is found that, when the melted fibers are deposited along a short border and a long border, respectively, in the same rectangular layer of the prototype (see Fig. 11), the warp deformation with the depositing path along the short border is much smaller than along the long border. The phenomenon can be explained by the curves in Fig. 7, which depicts the relations of the warp deformation to the stacking section length. Each layer of the prototype may be divided into some rectangular areas, and the extruded fiber is controlled to be deposited along the short border of these rectangular areas. This layer-area-distributing depositing strategy can greatly reduce the warp deformation.

(2) In the FDM process, it is found that the calculated deformation is always a little bigger than the actual deformation. According to the measurement of cubic specimens with different sizes, the actual deformation of the specimens is smaller by 2%~5% than the calculated deformation.

In the FDM process, a supporting structure is required to form a base to mount the prototype and to support any overhanging features. To begin with, about six base layers as a fiducial base are firstly deposited on the foam worktable. The base plane composed of six layers is firmly embedded in the foam worktable without any deformation. In addition, the prototype is enwrapped with the support structures. Due to the restriction of the support structures, the prototype has a little warp deformation in the fabrication process. At the same time, the prototype is fabricated in a closed chamber with a relatively high constant temperature, and it will still remain in the chamber for a while after the fabrication is finished. The process is so similar to an annealing process as to partially eliminate the thermal stresses of the prototype. In the post-processing

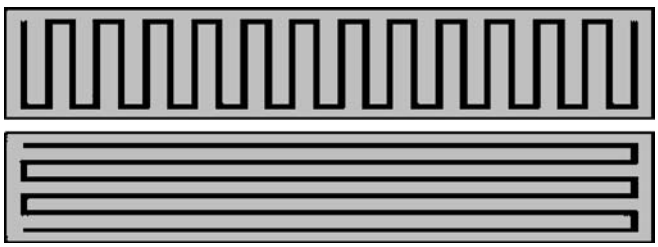

Fig. 11 Long raster and short raster deposition patterns: (*upper*) short raster pattern. (*lower*) long raster pattern

phase, the supports are manually removed by stripping them from the prototype surface. With the restriction of the worktable and the supports eliminated, the actual deformation due to the release of residual stresses becomes slightly smaller than the calculated deformation. This is the reason for the differences between the actual deformation and the calculated deformation.

4.3 Application case

Using the mathematical model as an analysis tool, combining with the above selection methods of the material and technical parameters for the reduction of deformation, a thin-wall and slender veil of a car lamp with size 284 mm×51 mm×38 mm (see Fig. 12) can be fabricated by the FDM2000 machine.

Material selection: ABS P400 filament was selected as a thermoplastic material due to its relatively small linear shrinkage rate.

Chamber temperature selection: Increasing the chamber temperature can effectively reduce the deformation of the FDM prototype. However, the body temperature of the FDM prototype will be also increasing with increasing chamber temperature, which can decrease the cooling speed of the deposition layer area. If the temperature of the deposited fiber has not decreased under the temperature of ABS P400's soft point of 105°C, a "crust" on the surface of the strand will not be formed before the next adjacent fiber is due to be deposited. A higher envelope temperature can cause deposited fiber rippling by softening the material and reducing its flexural modulus, which is especially obvious in the short path deposition. These factors will influence the layer deposition quality. Therefore, balancing warp deformation and layer deposition quality, the chamber temperature is ultimately increased from the original 70°C to the current 75°C.

The depositing direction of the CAD model (see Fig. 12) is selected with the help of the ratio table (see Table 1). The FDM system software QuickSlice builds the scanning road paths in each layer slice; in succession, the paths need to be manually revised with the reference of Table 1 and Fig. 11. According to the average deflection of the car lamp surface not exceeding 0.5 mm, the ratio of the stacking section length to the deposited layers thickness is required to be less than 6. The thin-wall and slender prototype of the car lamp is fabricated with the deposition direction as seen in Fig. 13, and the lamp surface is facing outward. Special support structures can be fabricated in the hollow of the car lamp to support any overhanging features. The supports may also fix the car lamp body in the fabricating process, which is helpful for the reduction of warp and twist deformation. In every layer slice, fibers will be deposited along the direction of the zig-zag path with an angle of 45° or −45° between the shorter line of the approximate rectangle slice and the depositing path. The directions of the deposition road paths between two adjacent layers are inter-vertical. For all of the layers of the lamp prototype, the ratio of the stacking section length to the deposited layers' thicknesses is controlled between 2.8 and 4.5. The calculated value of warp deformation is between 0.2 mm and 0.4 mm. Finally, the prototype of the car lamp has been successfully fabricated (see Fig. 14). Then, point cloud data of the prototype surface of the car lamp veil are acquired by an optical three-coordinate measuring machine. Comparing the point cloud data with the CAD model data, the actual

Fig. 13 FDM prototype of the car lamp veil with size 284 mm × 51 mm × 38 mm

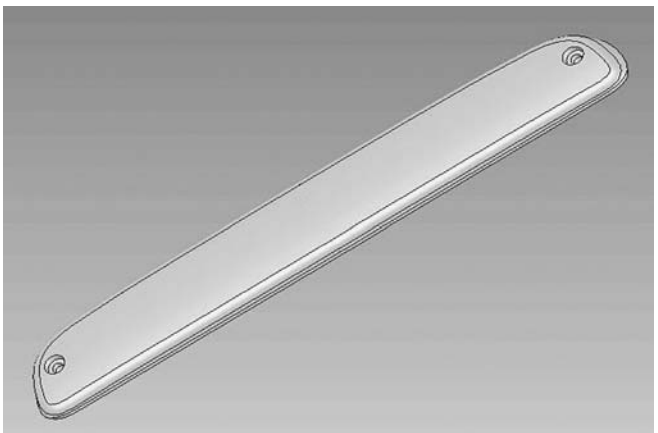

Fig. 12 CAD model of a car lamp veil with size 284 mm×51 mm×38 mm

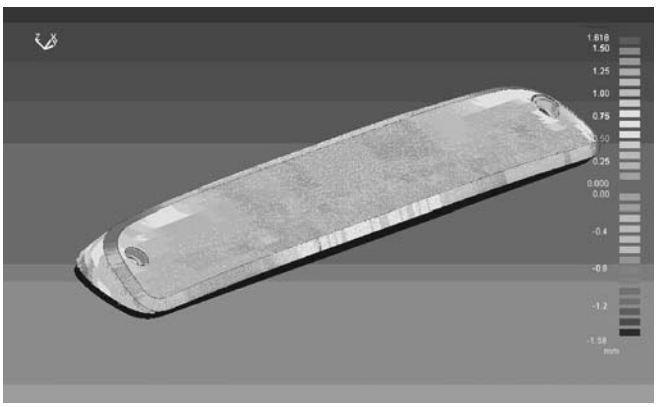

Fig. 14 The matching between the surface point cloud data of the lamp veil prototype and its surface from the CAD model data

average deflection of the prototype surface is 0.32 mm (see Fig. 14). The deflection just lies in the range of the calculated value. The fabrication effects are preferable, and reach the technical requirements. However, the mathematical model of warp deformation is discovered by the rectangular parallelepiped prototype. For the thin-wall prototype, due to the coupling action of warp deformation and twist deflection, residual stresses will centralize in some areas of the prototype. And the deformation will deviate largely from the calculating deformation value due to the release of residual stresses when the support structures are manually removed from the prototype's surface. Generally, the deviant deformations mainly lie on the joints of different curve surfaces. The maximum deformation of the car lamp prototype is 1.618 mm (see Fig. 14). The surface error lies on the central area of the joint between the car lamp face and the base fringe. Fortunately, the maximal deviation has little influence on the surface uniformity of the car lamp prototype. Through the post-processing procedures of surface finishing and polishing, the prototype can be used as a molding board to fabricate the silicon rubber mold for small-batch production of the car lamp veil.

5 Conclusions

Warp deformation is an important index to evaluate the quality of a fused deposition modeling (FDM) prototype. The deformation of the FDM prototype is influenced by some factors. These factors include the material characteristics, setup of the fabrication parameters, geometrical structure of the CAD model, and deposition path planning. Through three points of reasonable hypotheses about the FDM process, the mathematical model of the warp deformation is discovered for the first time. At the same time, each of the influencing factors, including the deposition layers number n, the stacking section length L, the chamber temperature T_e, and the material linear shrinkage rate α, is quantitatively analyzed. The mathematical model can provide a scientific tool for controlling and adjusting the deformation. Based on the conclusions of the model analysis, some issues and phenomena in the FDM process are rationally explained. Furthermore, some improving methods for the effective reduction of the prototype warp deformation are proposed. From a prototype case of a car lamp veil, the applying effect is better.

Acknowledgement This work is supported by the Shanghai Automobile Development Foundation (grant no: 0330).

References

1. Jayanthi S, Keefe M, Gargiulo EP (1994) Studies in stereolithography: influence of process parameters on curl distortion in photopolymer models. In: Proceedings of the Solid Freeform Fabrication Symposium, Austin, Texas, August 1994, pp 250–258
2. Yang H-J, Hwang P-J, Lee S-H (2002) A study on shrinkage compensation of the SLS process by using the Taguchi method. Int J Mach Tools Manuf 42(11):1203–1212
3. Nickel AH, Barnett DM, Prinz FB (2001) Thermal stresses and deposition patterns in layered manufacturing. Mater Sci Eng: A 317(1–2):59–64
4. Sonmez FO, Hahn HT (1998) Thermomechanical analysis of the laminated object manufacturing (LOM) process. Rapid Prototyping J 4(1):26–36
5. Detlef K, Chua CK, Du ZH (1999) Rapid prototyping issues in the 21st century. Comput Ind 39(1):3–10
6. Wu S (1982) Polymer interface and adhesion. Marcel Dekker, New York
7. Rodriguez JF, Thomas JP, Renaud JE (2000) Characterization of the mesostructure of fused-deposition acrylonitrile-butadiene-styrene materials. Rapid Prototyping J 6(3):175–185
8. Yardimci AM (1999) Process analysis and planning for fused deposition. PhD thesis, University of Illinois at Chicago, Illinois